Tempered martensite embrittlement: Role of retained austenite and cementite

H. K. D. H. Bhadeshia and D. V. Edmonds

The microstructural and property changes accompanying the tempering of quenched low-alloy steels have been examined and correlated with the tempered martensite embrittlement (TME) phenomenon. TME was detected in an Fe–C–Mo steel and found to be controlled by the relatively coarser intralath cementite, rather than by the interlath cementite resulting from the decomposition of $<2\%$ retained austenite present as films between the martensite laths. In an Fe–C–V steel containing about 5% interlath retained austenite, TME was controlled by coarsening of the comparatively larger amount of interlath cementite resulting from thermal decomposition of the interlath retained austenite. In both cases fracture was translath, consistent with the crack nucleation role of cementite rather than that of providing an easy fracture path. In an Fe–C–Mn–Si steel containing negligible retained austenite and fine carbides TME was not found. Furthermore, embrittlement could not be associated with the transition from ε-carbide to cementite.

Manuscript received 15 September 1978: in final form 9 January 1979. H. K. D. H. Bhadeshia, BSc, and D. V. Edmonds, MA, BSc, PhD, are in the Department of Metallurgy and Materials Science, University of Cambridge.

Tempered martensite embrittlement (TME) is characterized by a loss in toughness accompanying the tempering of martensitic structures at temperatures generally in the vicinity of 350°C.[1-3] TME is not conceptually connected to any of the more usual temper embrittlement phenomena involving impurity segregation; failure is distinctively transgranular with respect to the prior austenite grains.[1,3-5] McMahon and Thomas[2] first correlated the thermal decomposition of interlath retained austenite (and resultant formation of interlath cementite films) with a drop in toughness upon tempering. Thomas[1] further considered that the thermal instability of interlath austenite is a fairly general cause of TME and showed that the failure to detect any interlath retained austenite in Fe–Mo–C alloys[1,6] correlated with the apparent absence of TME in these steels. Horn and Ritchie[3] have extended this idea by proposing that TME in pure* steels is caused by the combined effect of both the thermal and mechanical instability of interlath retained austenite. Meanwhile, King *et al.*[5] obtained TME in a plain carbon steel when the fracture mode was transgranular cleavage over a range of tempering temperatures and attributed TME simply to the coarsening of interlath cementite.

There is also some controversy as to the exact role of the interlath cementite in the embrittlement process. Rao and Thomas[4] consider the fracture path during TME in pure* steels to be interlath along the cementite films resulting from the thermal decomposition of retained austenite; Horn and Ritchie[3] also support the possibility of interlath failure, although in both cases little metallographic evidence has been presented. On the other hand, there appears to be ample evidence for failure which is transgranular with respect to both the prior austenite grains and the martensite laths.[5,7-10]

In view of the above uncertainty surrounding recent studies of TME, a detailed examination of structural changes accompanying the tempering of a series of steels was undertaken in order to correlate these changes with any embrittlement phenomena observed.

EXPERIMENTAL PROCEDURE

The experimental alloys used were prepared from high-purity base materials as 20 kg vacuum induction melts. The ingots were forged and hot rolled to 10 mm diameter rod followed by a hot-swage reduction to 8 mm diameter rod. The compositions are listed in Table I.

The Fe–Mo–C and Fe–V–C steels were austenitized at 1200°C for 15 min, while the Fe–Mn–Si–C alloy was austenitized at 1080°C for 10 min prior to quenching into water at ambient temperature. Austenitizing and tempering treatments were carried out in tube furnaces. The specimens were protected by a proprietary coating together with a dynamic argon atmosphere.

The impact specimens used were 8 mm in diameter and 45 mm long with a 1 mm deep notch. The notch was machined (prior to any heat treatment) with a standard Hounsfield notching tool but with the specimen supported in a jig with an eccentricity of 3·5 cm. *In situ* hot impact testing was facilitated by jets of furnace-heated air directed at the specimen. A thermocouple attached directly to the specimen in the vicinity of the notch enabled the continuous monitoring of temperature.

Transmission electron microscopy was carried out using a Philips EM300 microscope operated at 100 kV. Thin foils were prepared directly from discs machined from impact specimens such that the foil plane was normal to the axis of

* i.e. embrittlement not impurity controlled.

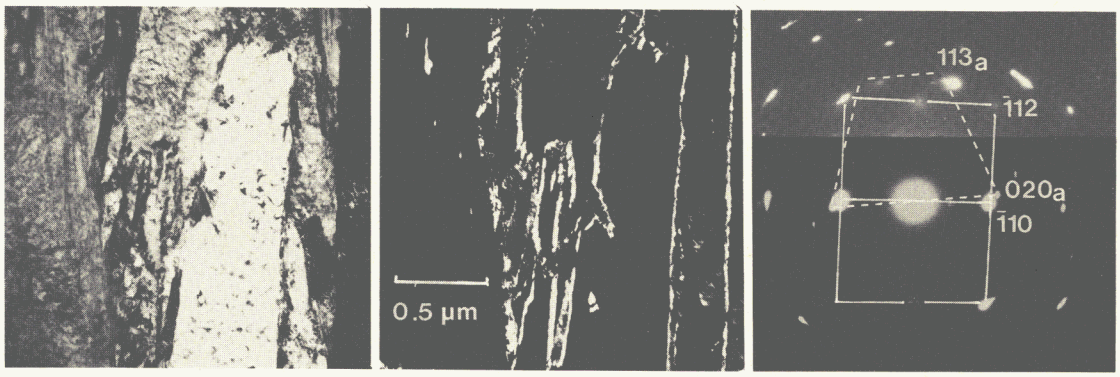

(a) (b) (c)

1 Transmission electron micrographs of austenitized and quenched Fe–2Mo–0·2C alloy: (a) bright-field image, (b) retained austenite dark-field image, (c) corresponding diffraction pattern.

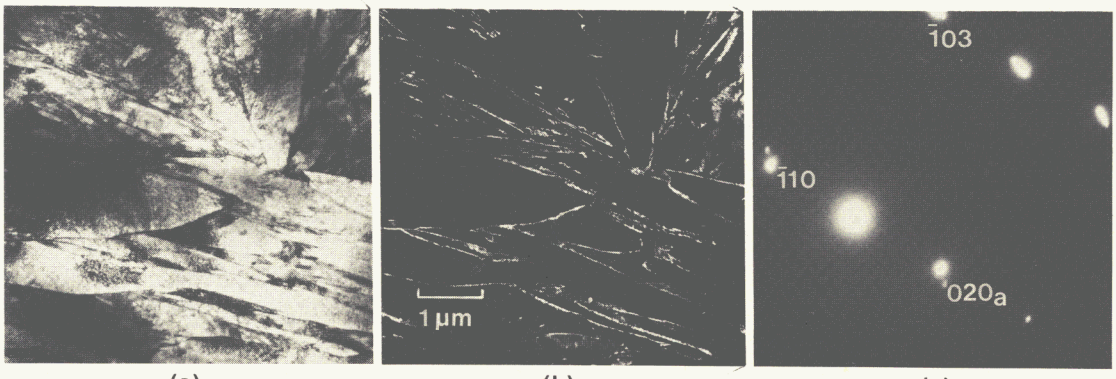

(a) (b) (c)

2 Transmission electron micrographs of austenitized and quenched Fe–4Mo–0·2C alloy: (a) bright-field image, (b) retained austenite dark-field image, (c) corresponding diffraction pattern.

the swaged rod. Foil preparation was on a jet polisher using an electrolyte of 25% glycerol, 5% perchloric acid, and 70% ethanol at a polishing voltage of 55 V and at room temperature.

Fractography was conducted on a Cambridge Stereoscan scanning electron microscope operated at 30 kV.

Retained austenite determinations were carried out on a Philips horizontal X-ray diffractometer using Co radiation and with a LiF crystal monochromator in the diffracted beam. The X-ray lines used to determine the proportion of austenite were $\{022\}_\gamma$, $\{113\}_\gamma$, $\{112\}_\alpha$, and $\{022\}_\alpha$.

RESULTS AND DISCUSSION

Fe–Mo–C alloys

Detailed electron microscopy and electron diffraction analysis (Figs. 1 and 2) revealed retained austenite in both Fe–2Mo–0·2C and Fe–3·9Mo–0·18C directly quenched alloys. The austenite was found to be stable even after refrigeration at −196°C for 1 h (Fig. 3). It is estimated that the volume fraction of retained austenite is less than 0·02 since X-ray analysis failed to detect convincingly any austenite. These results disagree with those of Clark and Thomas[1,6] who did not detect any retained austenite in Fe–Mo–C alloys of similar composition. This disagreement possibly reflects the difficulties associated with the detection of films of retained austenite in thin foils of as-quenched samples. Thomas[1] has delineated several of these difficulties. However, other factors may also be involved. The fact that thin films of retained austenite are observed in a variety of high M_s temperature alloys is surprising at first sight, particularly since there is no partitioning of carbon into this austenite.[11] Furthermore, the observations are in thin foils where the austenite would be expected to be even more unstable because of the removal of bulk constraints. Hence, if it is assumed that further transformation of the film austenite would involve movement of extant

Table I Alloy compositions, wt-%

	C	Mn	Si	Mo	V	S	P
Fe–Mn–Si–C	0·43	3·00	2·02	—	—	0·002	0·002
Fe–V–C	0·25	—	—	—	1·08	0·012	0·004
Fe–4Mo–C	0·18	—	—	3·90	—	—	—
Fe–2Mo–C	0·20	—	—	2·0	—	—	—

Dash indicates not determined.

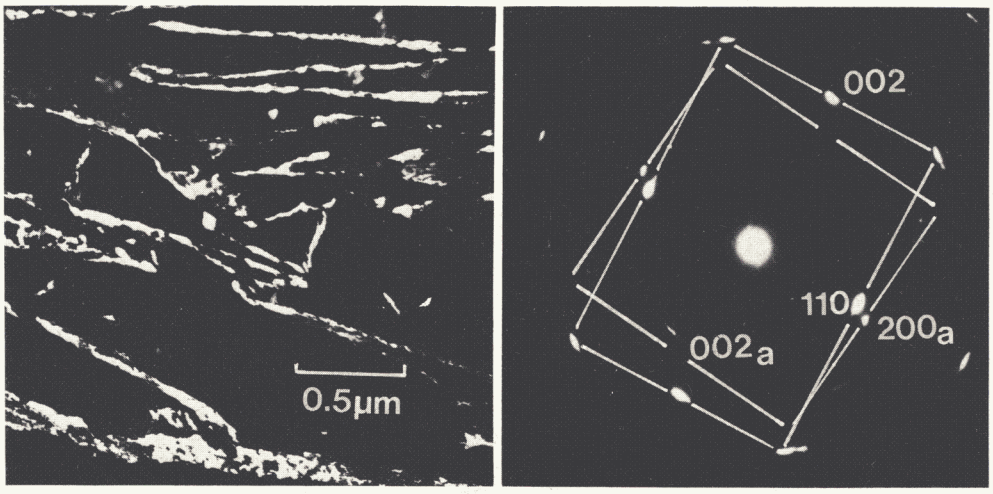

3 (a) Retained austenite dark-field image and (b) corresponding diffraction pattern from austenitized and quenched Fe–4Mo–0·2C alloy following refrigeration at −196°C for 1 h.

martensite/austenite interfaces, then a possible stability criterion could be that a major component of the martensite transformation displacement vector must lie in the foil plane such that a significant constraint effect is still experienced by the austenite. Hence the foil orientation with respect to the displacement directions concerned may be of importance. The influence of bulk crystallographic texture may then also be of relevance to the stability of the austenite, not only in bulk specimens, but also in thin foils. Recent work by Bhadeshia and Edmonds[12] has shown a clear relationship between the volume fraction of bainitic retained austenite and the $\{111\}_\gamma$ texture. It is therefore possible that such variations might account for the detection differences between the specimens examined in the present work (from 8 mm swaged rod) and in that of Clark and Thomas (from 13 mm rolled plate).

Using the Fe–3·9Mo–0·18C alloy, impact tests were carried out over a range of testing temperatures (Fig. 4) and it was found that there was an almost monotonic decrease in toughness relative to the as-quenched specimens with increasing tempering temperature. This is despite the continuous decrease in hardness with increasing tempering temperature (Fig. 5). It is therefore clear that an embrittling mechanism is operating even though a well defined TME trough is not obvious.

Transmission electron microscopy revealed considerable intralath cementite precipitation in the specimen tempered at 190°C (Fig. 6(*a*)). The lath boundaries did not reveal any cementite precipitation although retained austenite could be detected readily (Fig. 6(*b*) and (*c*)). Consequently, as the toughness was reduced by this tempering treatment it can only be concluded that in this alloy it is the intralath cementite that is responsible for the embrittling effect.

Raising the tempering temperature to 295°C led to the decomposition of the interlath retained austenite to give cementite films. However, the cementite films appeared to be discontinuous (Fig. 7), which is not surprising in view of the fact that they arise from austenite films only a few hundred angstroms thick. The cementite probably nucleates at several positions of the austenite/martensite interface (Bhadeshia and Edmonds[12] have found this to be the case with thicker films of bainitic retained austenite) so that the final decomposition product is small discrete cementite particles at the interlath boundary. Figure 7 also shows that

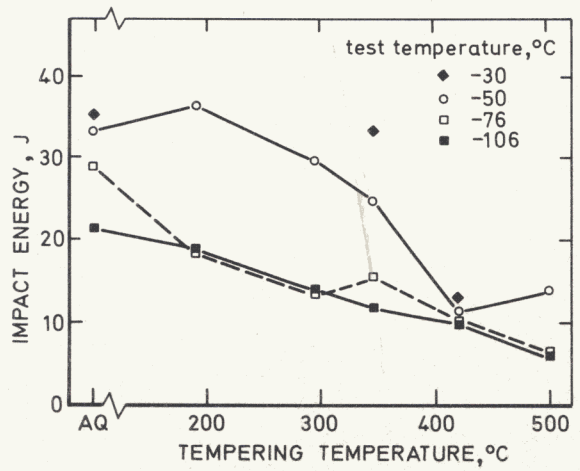

4 Results of impact tests on Fe–4Mo–0·2C alloy.

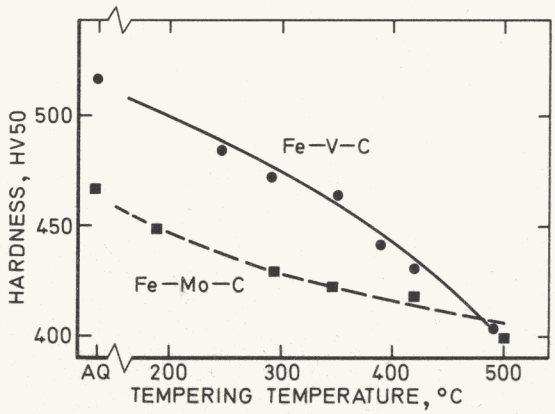

5 Variation of hardness with tempering temperature for Fe–4Mo–0·2C and Fe–1V–0·2C alloys.

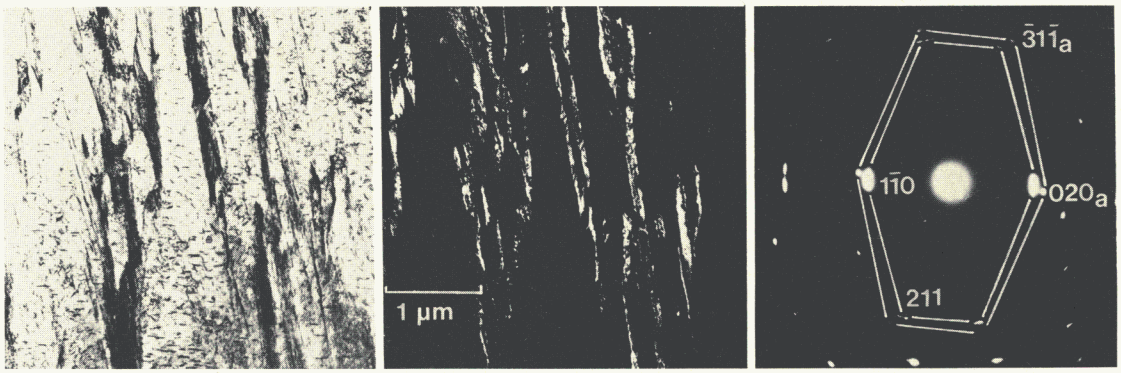

(a) (b) (c)

6 Transmission electron micrographs of Fe–4Mo–0·2C alloy after quenching and tempering at 190°C for 1 h: (a) bright field image, (b) retained austenite dark field image, (c) corresponding diffraction pattern.

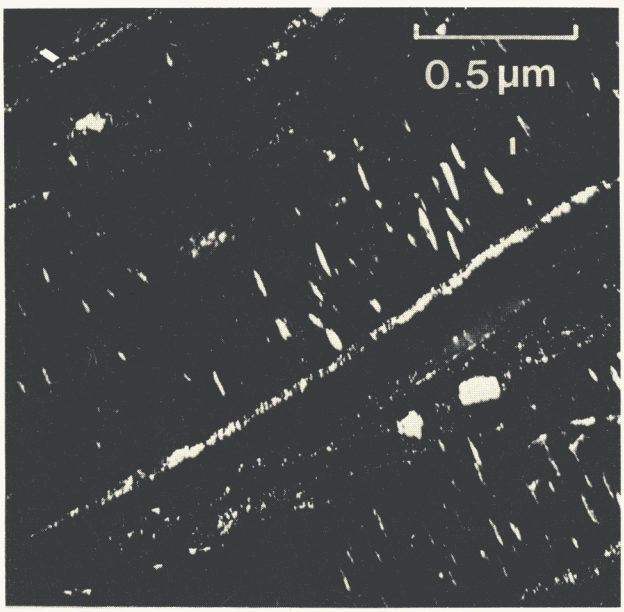

7 Cementite dark-field image using $(103)_\theta$ reflection from Fe–4Mo–0·2C alloy after quenching and tempering at 295°C for 1 h.

the interlath cementite adopts an orientation relationship with the martensite matrix which is equivalent to one of the intralath cementite variants. This is consistent with the formation of the cementite in contact with both martensite and austenite at the interface, such that the orientation variant which is favoured is the one with low energy orientations with respect to both austenite and martensite.

Hence, during the earlier stages of tempering when retained austenite has not yet decomposed to interlath cementite, TME is clearly controlled by intralath cementite. Even at 295°C, the initial interlath cementite resulting from the thermal decomposition of retained austenite (i.e. prior to the onset of significant coarsening) is less coarse relative to intralath carbides. At a tempering temperature of 420°C, coarsening of interlath cementite was observed (Fig. 8) and it is possible that this could then exercise control of TME. The overall tempering behaviour is therefore consistent with the wide TME trough found. Indeed, even the as-quenched martensite probably may not be at optimum toughness due to slight autotempering.

Of the specimens tested at −76°C, scanning electron microscopy revealed that only the as-quenched specimen had any ductile component of failure, while all specimens

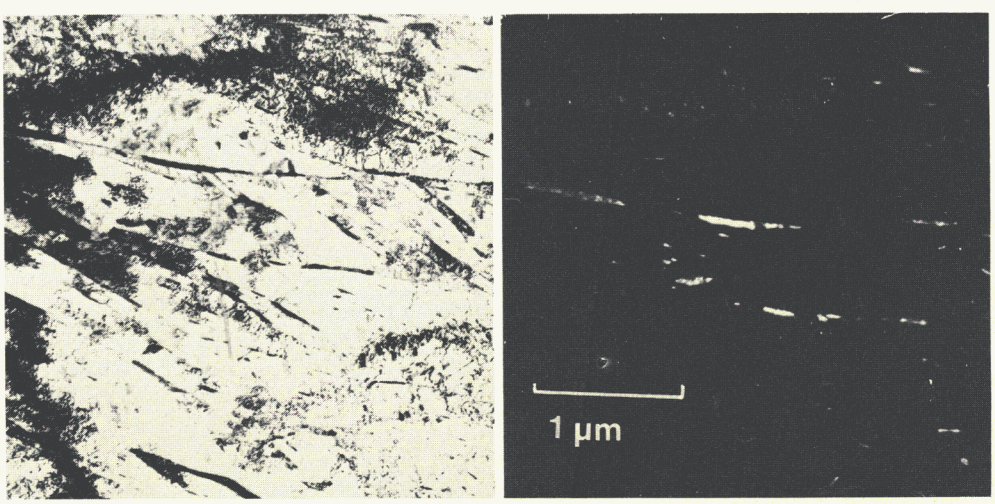

(a) (b)

8 Transmission electron micrographs of quenched Fe–4Mo–0·2C alloy after tempering at 420°C for 1 h: (a) bright-field image, (b) cementite dark-field image using $(113)_\theta$ reflection.

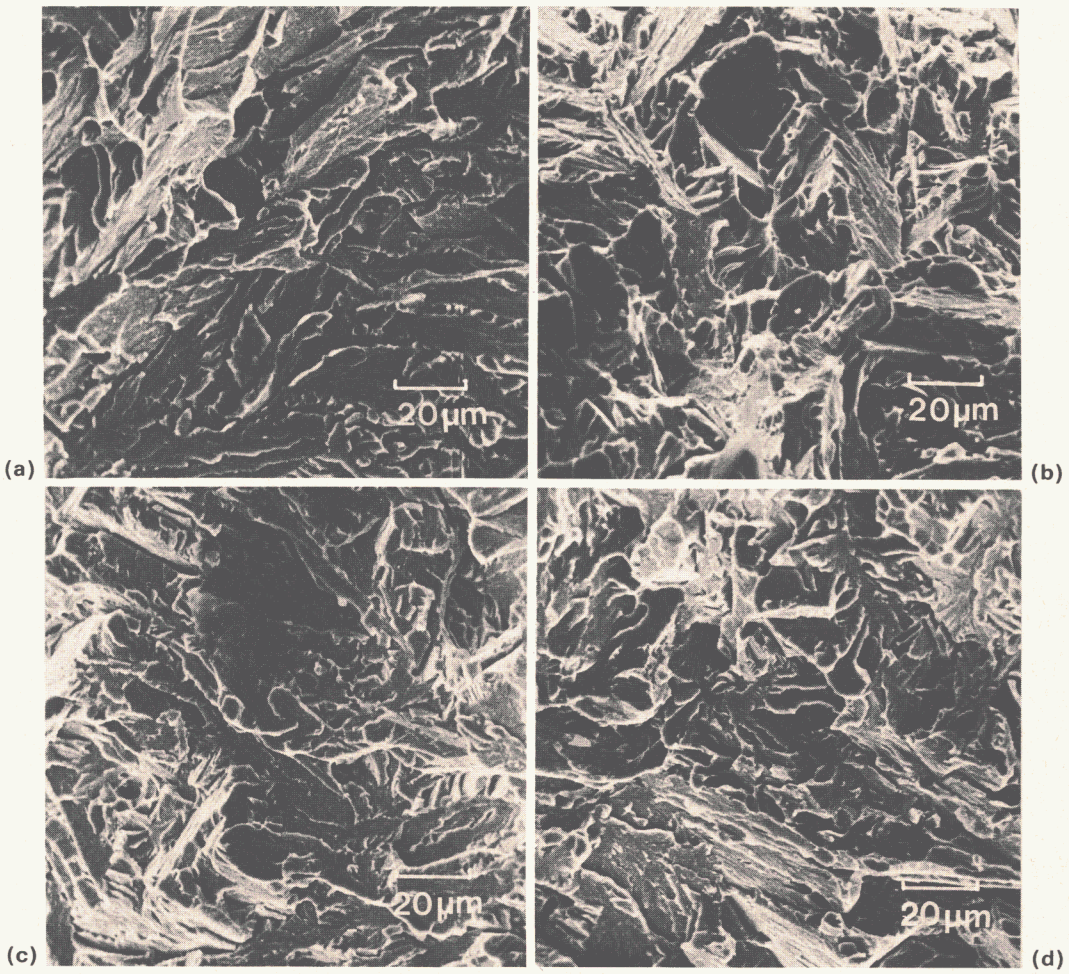

9 Typical fractographs showing cleavage fracture following impact tests at −106°C in Fe–4Mo–0·2C alloy: (a) as-quenched, (b) quenched and tempered at 190°C for 1 h, (c) quenched and tempered at 295°C for 1 h, (d) quenched and tempered at 420°C for 1 h.

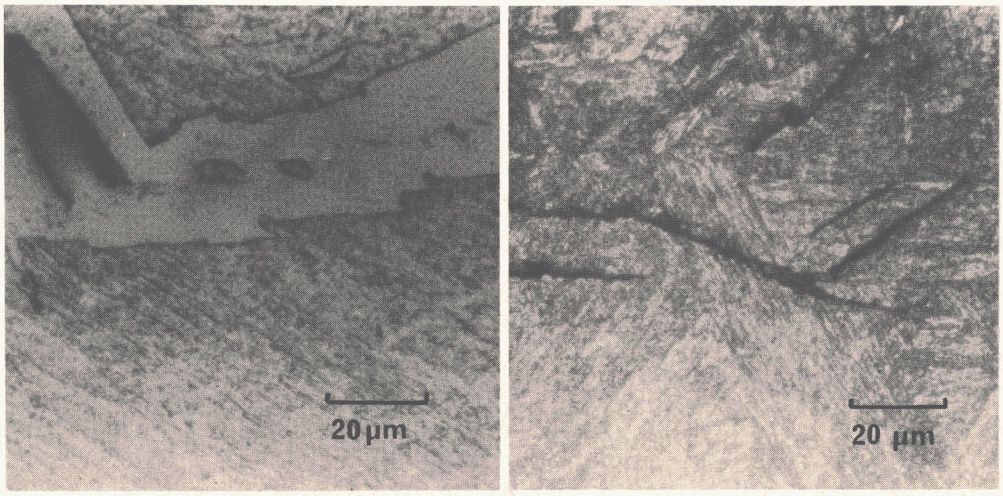

10 Fe–4Mo–0·2C alloy quenched and tempered at 420°C for 1 h followed by impact fracture at −106°C: (a) optical micrograph of nickel-plated fracture surface, (b) optical micrograph of internal secondary cracks.

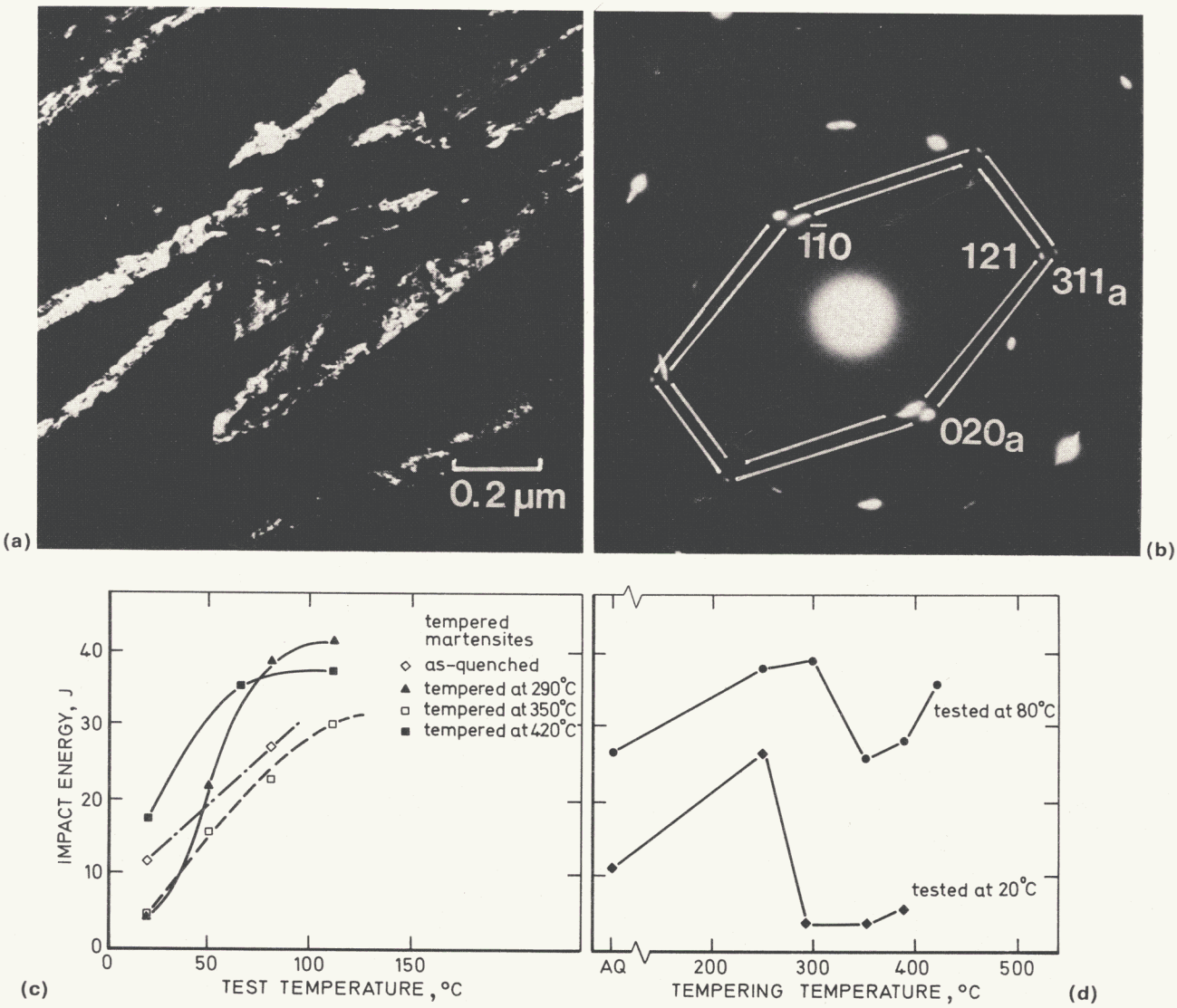

11 (a) Retained austenite dark-field image and (b) corresponding diffraction pattern from austenitized and quenched Fe–1V–0·2C steel. (c) and (d) Results of impact tests on Fe–1V–0·2C steel.

tested at −106°C exhibited cleavage fracture (Fig. 9). Despite this fact, embrittlement (relative to the as-quenched specimen) is still observed and this is consistent with a cementite coarsening mechanism for TME.[5] The fact that there is no rise in impact energy at −106°C at the highest tempering temperatures is probably an indication of the possible insensitivity of the cleavage strength to the plastic yield strength, indicating that little localized plastic deformation must be occurring in association with cleavage in this alloy.

Optical examination of a nickel-plated fracture surface of a specimen in the most brittle condition revealed that the main cleavage fracture path (and that of internal secondary cracks) was, in general, translath (Fig. 10). The internal cracks examined were near the fracture surface and approximately parallel to the main fracture path. The benefit of examining secondary cracks, as well as the main crack, is that the microstructure on both sides of the crack can be observed. These observations indicate the crack nucleation role of cementite rather than the provision of an easy fracture path.

At first sight, the present embrittlement results contradict those of Clark and Thomas,[1,6] who claim an absence of any TME effect (or retained austenite) in Fe–Mo–C steels. However, closer examination of the toughness results for their alloy designated C-198 (Fe–0·18C–0·38Mn–0·15Si–3·85Mo, Ref. 6) shows that specimens tempered at 400°C have a lower toughness than as-quenched specimens, despite their lower yield stress.

Fe–1·08V–0·25C alloy

Tests similar to those on the Fe–Mo–C alloy were carried out on the Fe–V–C alloy which is known to exhibit interlath films of retained austenite[13] (Fig. 11(*a*) and (*b*)). Figure 11(*c*) and (*d*) illustrates the results obtained. It is clear that the TME trough in this steel is well defined as compared to the Fe–Mo–C steel, although it is noted that the test temperature ranges are different, owing to the differing impact transition temperatures. The Fe–V–C alloy contains about 5% interlath retained austenite, as indicated by X-ray analysis. Upon tempering the quenched structure at 290°C transmission electron microscopy showed that the

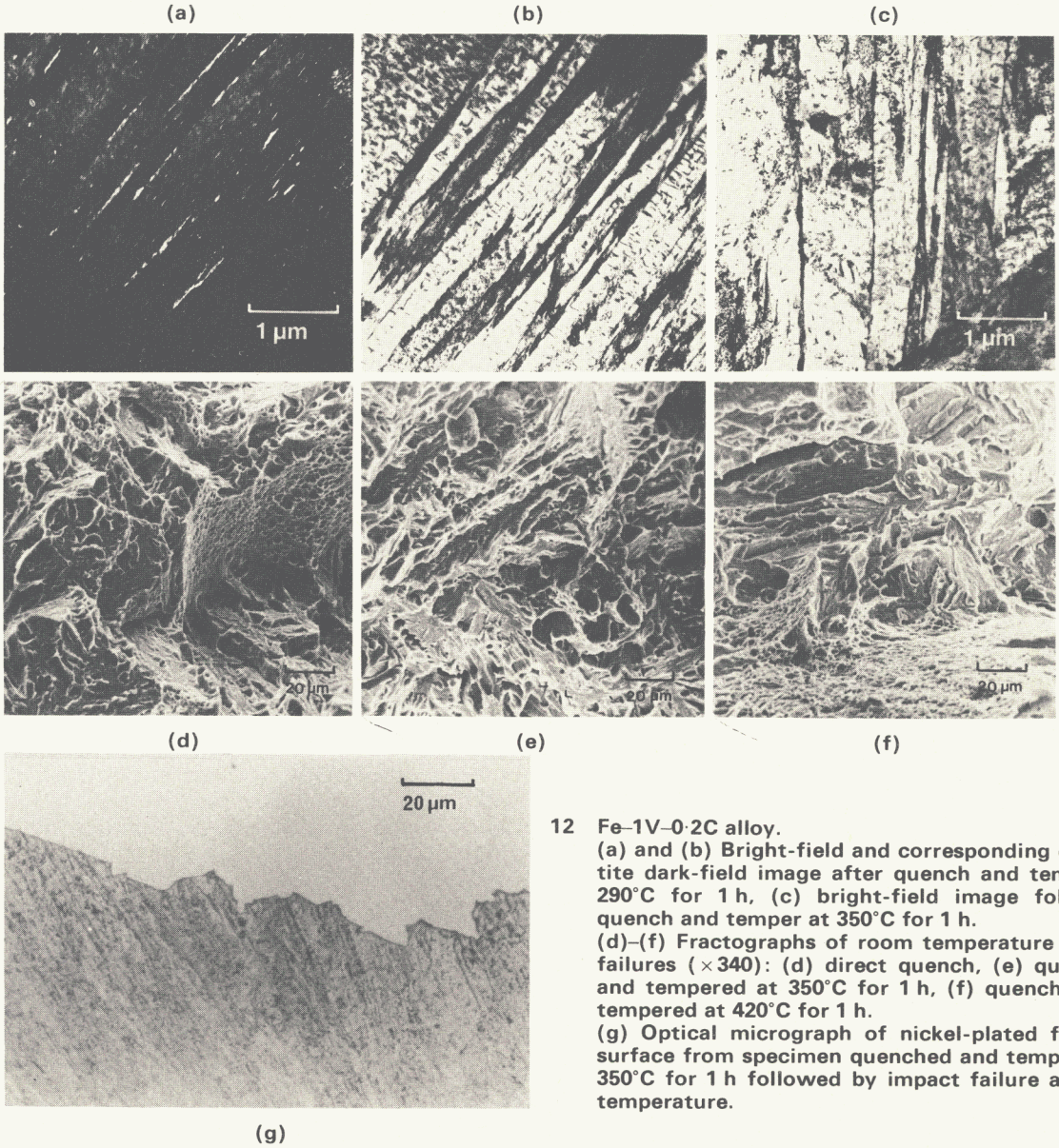

12 Fe–1V–0·2C alloy.
(a) and (b) Bright-field and corresponding cementite dark-field image after quench and temper at 290°C for 1 h, (c) bright-field image following quench and temper at 350°C for 1 h.
(d)–(f) Fractographs of room temperature impact failures (×340): (d) direct quench, (e) quenched and tempered at 350°C for 1 h, (f) quenched and tempered at 420°C for 1 h.
(g) Optical micrograph of nickel-plated fracture surface from specimen quenched and tempered at 350°C for 1 h followed by impact failure at room temperature.

austenite had decomposed into laths of cementite at the martensite boundaries (Fig. 12(*a*) and (*b*)). At 350°C, well within the TME trough, limited coarsening of the interlath cementite was detectable (Fig. 12(*c*)). Despite the fact that the retained austenite had decomposed completely at 290°C, the impact curves show that this treatment does not *fully* embrittle the steel; the embrittlement is more complete after tempering at 350°C. Since the interlath cementite is coarser than the intralath cementite in this steel (presumably because of the relatively larger amount of retained austenite) it is concluded that it is the coarsening of interlath cementite that is responsible for TME rather than the decomposition of the retained austenite itself.

While the fracture mode (at room temperature) was mainly quasi-cleavage following the 350°C tempering, the as-quenched and 420°C tempered specimens showed large amounts of dimpled rupture as well (Fig. 12(*d*)–(*f*)). Furthermore, in this alloy where interlath cementite controls TME, the nickel-plated fracture surface of the specimen in the most brittle condition revealed *translath* failure (Fig. 12(*g*)), indicating once again the crack nucleation role of cementite rather than the provision of any easy fracture path. It should be noted that the mechanical instability of retained austenite has no role in either of the above steels examined since not only is embrittlement present in the absence of retained austenite (following tempering) but the embrittled toughness values fall below those of the as-quenched specimens.

Fe–0·43C–3·0Mn–2·02Si

The low M_s temperature (dilatometrically measured to be 220°C) and the high silicon content of the Fe–C–Mn–Si steel give carbide-free supersaturated martensite when directly quenched from the austenitized condition.[12] The tempering of this martensite is easy to follow, partly because of the effect of silicon in retarding cementite precipitation. Tempering results predominantly in a fine dispersion of intralath carbides. Additionally, almost no retained austenite was detectable in the as-quenched condition, either by X-ray diffraction or by transmission electron

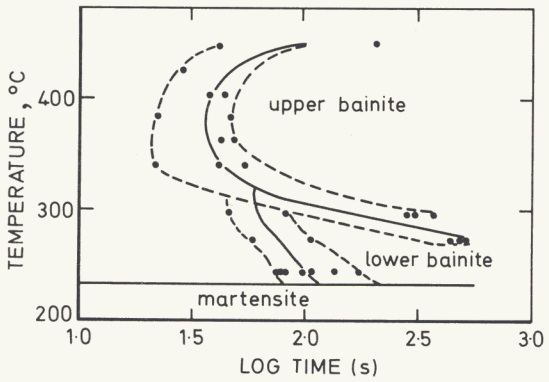

(a)

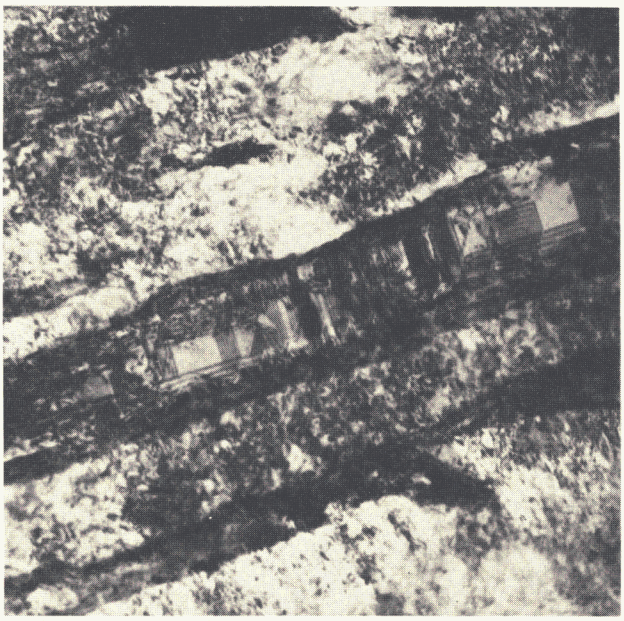

(b)

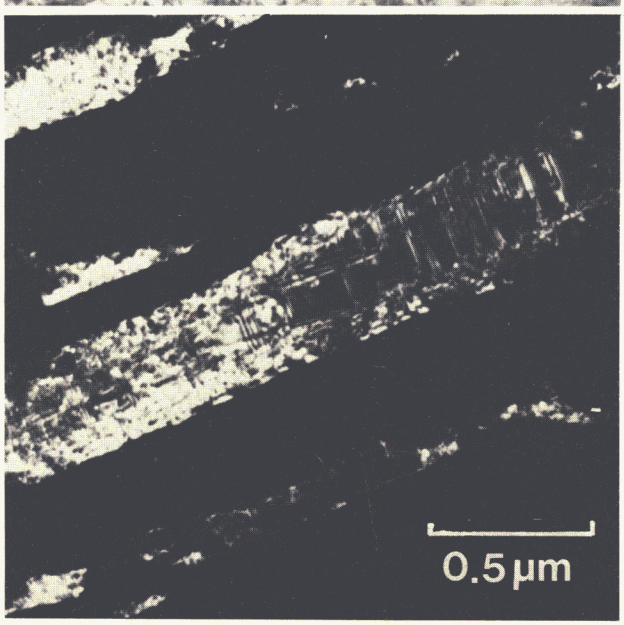

(c)

13 (a) 5% TTT curve for Fe–Mn–Si–C steel. Region between dashed lines represents scatter observed. (b) Transmission electron micrograph of upper bainite formed by isothermal transformation at 350°C for 18 h, (c) corresponding retained austenite dark-field image.

microscopy. However, in view of the previously noted difficulties involved in austenite detection, it was decided to carry out more conclusive experiments.

Bhadeshia and Edmonds[12] have used this experimental steel in an examination of the bainite reaction and have extensively characterized its microstructure: the upper bainite in this steel consists of carbide-free bainitic ferrite and carbon-enriched retained austenite. The *TTT* diagram and a representative micrograph of the upper bainitic structure is reproduced in Fig. 13. With the help of this information, a specimen was partially transformed to martensite (by quenching to a temperature below M_s but well above 'M_f') followed by an up-quench into the upper bainitic region so that the non-martensitic component of the specimen transformed to bainitic ferrite with carbon-enriched austenite.* Hence by illuminating the upper bainitic austenite (UBA) in a single prior austenite grain in dark field it was possible to ensure that any austenite in the martensite regions in the same prior austenite grain was also illuminated. By using the UBA reflection and observing the martensitic regions in dark field it was shown conclusively that the martensitic regions contained negligible amounts of retained austenite. Figure 14 shows adjacent bainitic and martensitic regions with retained austenite illuminated only in the bainite.

The results of impact tests on this alloy in the as-quenched and tempered condition are illustrated in Fig. 15. Curve A represents the as-quenched martensite. The specimens of Curve B contain martensite with ε-carbide positively identified by electron diffraction (Fig. 16) following tempering at 245°C for 15 min. Comparison with as-quenched martensite shows that there is a small but significant decrease in toughness of the tempered martensite in the region of ductile failure (upper shelf). This effect is also reflected in the fall-off of the as-quenched transition curve at the highest testing temperatures since *in situ* tempering of the specimen occurs during impact testing. This toughness loss, despite the reduced hardness of the tempered martensite, is probably caused by an increased capacity for void nucleation in the specimens containing ε-carbide. After tempering at 355°C for 4 h, the ε-carbide was replaced by cementite (Fig. 17) but this in itself has clearly caused no TME. Further tempering led to complete precipitation of cementite with the concurrent elimination of ε-carbide. The cementite dispersion is noticeably refined by the silicion addition. The results show that there is no characteristic TME in this steel of a form similar to that in Fe–Mo–C or Fe–V–C alloys. This is entirely consistent with the absence of any coarse cementite or interlath retained austenite (with its attendant decomposition product of interlath cementite).

GENERAL SUMMARY

By the critical examination of a selected series of steels it proved possible to characterize the TME phenomenon in terms of the detailed microstructural changes accompanying tempering, and in particular, to distinguish between the various controlling factors in different steels.

In the Fe–Mo–C steels less than 2% retained austenite was detected together with an extensive embrittlement effect relative to the as-quenched specimens. It was, however,

* It is noted that upper bainitic retained austenite in this alloy is completely stable with respect to the martensite reaction and remains stable even in a thin foil. It is enriched in carbon to the extent of about 2% and has an extensive defect structure.[12]

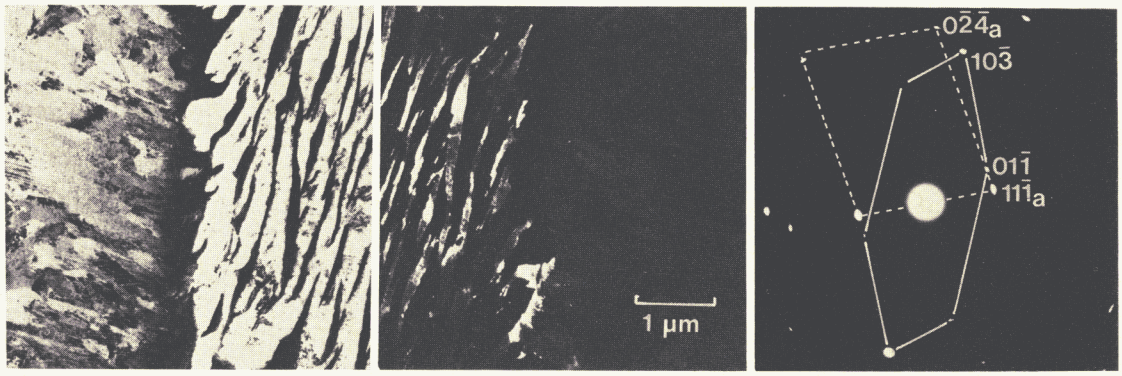

(a) (b) (c)

14 Transmission electron micrographs of Fe–Mn–Si–C alloy austenitized, quenched to 200°C, held at 200°C for 15 s and immediately up-quenched to 330°C, isothermally transformed for 1 h: (a) bright-field image, (b) retained austenite dark-field image, (c) corresponding diffraction pattern from the bainitic region.

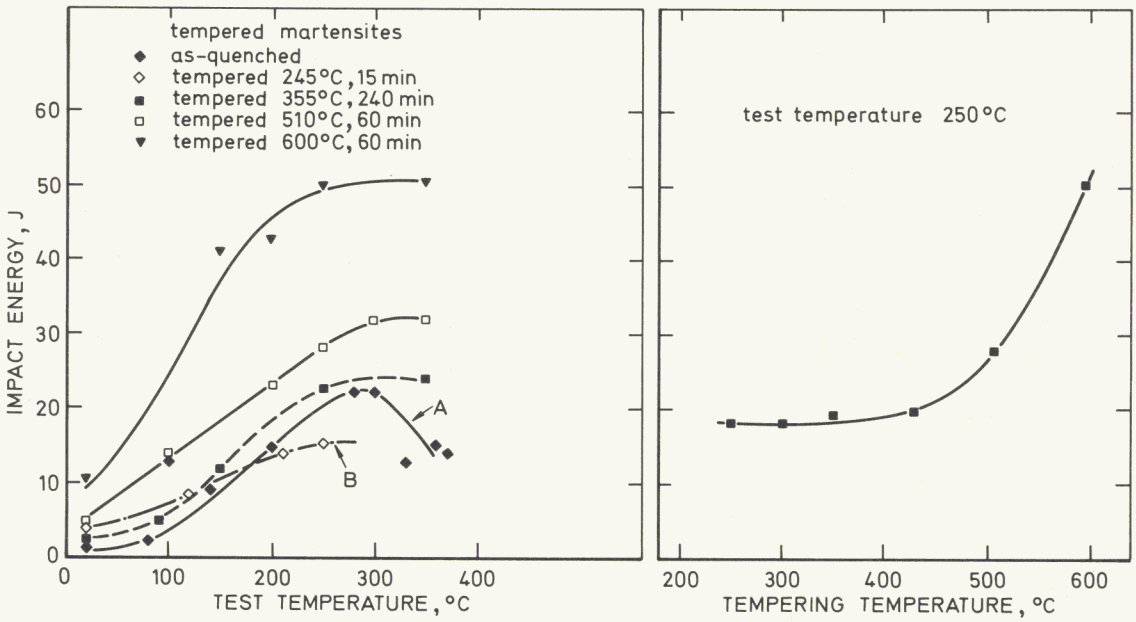

15 Results of impact tests on Fe–Mn–Si–C alloy.

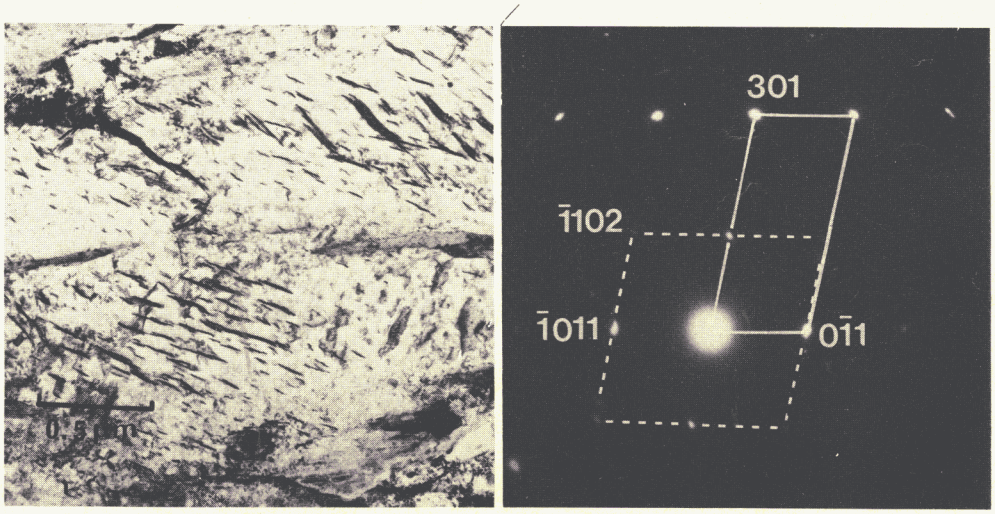

(a) (b)

16 (a) Transmission electron micrograph of quenched Fe–Mn–Si–C alloy after tempering at 245°C for 15 min. ×28 000. (b) Corresponding diffraction pattern.

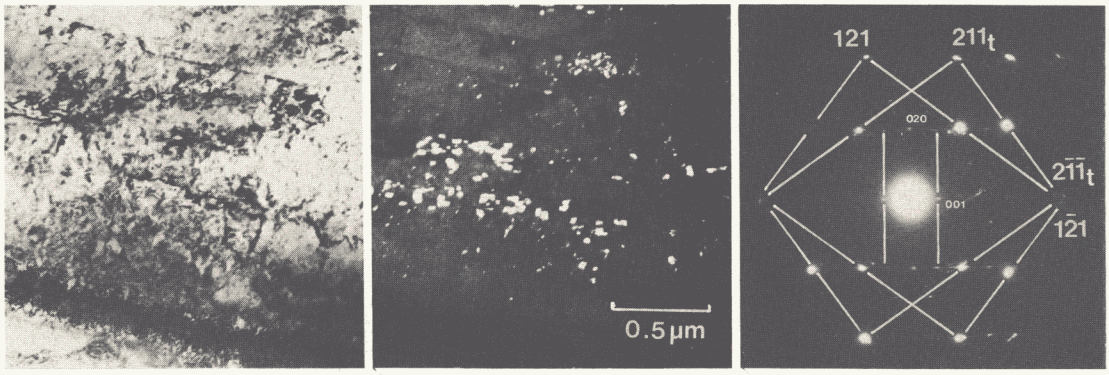

(a) (b) (c)

17 (a) Transmission electron micrograph of quenched Fe–Mn–Si–C alloy after tempering at 355°C for 4 h, (b) corresponding cementite dark-field image, (c) corresponding diffraction pattern showing cementite (small figures) simultaneously in Bagaryatski orientation with adjacent twin-related laths.

found that the coarser *intralath* cementite exercised the controlling influence on TME, and not the retained austenite or its subsequent decomposition product, namely a finer dispersion of interlath cementite.

The Fe–V–C steel contained substantially more retained austenite (about 5%) and in this case the TME could be attributed to the coarsening of interlath cementite formed during decomposition of this austenite. With this embrittlement mechanism the TME trough was well defined. Failure in both of these cases was found to be translath and this is consistent with the crack nucleation role of cementite in TME.

In the Fe–Mn–Si–C steel where the almost complete absence of retained austenite gave a structure containing only intralath carbides (which were extremely fine because of the high silicon level) no TME was detected and this is consistent with a TME mechanism based on the coarsening of cementite. Furthermore, no embrittlement could be attributed *per se* to the transition from ε-carbide to cementite.

With regard to the influence of silicon on carbide precipitation it would be of interest to modify the Fe–Mo–C and Fe–V–C steels with silicon in order to enhance tempering resistance.

The extent of the TME effect with respect to tempering temperature is important since there are conflicting requirements of a low tempering temperature (consistent with high strength requirements) and the need to be beyond the TME trough. While ideally TME should be eliminated, another approach might involve modifications such that the TME trough would be extremely narrow and well defined. In this respect, the interlath dependence of TME is more desirable, as in the Fe–V–C steel.

ACKNOWLEDGEMENTS

The authors are grateful to Professor R. W. K. Honeycombe for the provision of laboratory facilities and for his encouragement during the course of this work, and to the Ministry of Defence (RARDE), Fort Halstead, for their financial support. DVE also wishes to thank the Royal Society for the Warren Research Fellowship.

REFERENCES

1. G. THOMAS: *Metall. Trans.*, 1978, **9**, 331.
2. J. McMAHON and G. THOMAS: 'Microstructure and design of alloys', vol. 1, p. 180. **1974:** London (Metals Society).
3. R. M. HORN and R. O. RITCHIE: *Metall. Trans.*, to be published.
4. R. V. N. RAO and G. THOMAS: *Int. J. Fracture*, 1977, **13**, 705.
5. J. E. KING, R. F. SMITH, and J. F. KNOTT: Fracture 77, vol. 2, ICF4, Waterloo, Canada, 1977, pp. 279–286.
6. R. A. CLARK and G. THOMAS: *Metall. Trans.*, 1975, **6**, 969.
7. J. E. KING, R. F. SMITH, and J. F. KNOTT: *Int. J. Fracture*, 1977, **13**, 877.
8. U. H. LINDBORG and B. L. AVERBACH: *Acta Metall.*, 1966, **14**, 1583.
9. R. E. DOLBY and J. F. KNOTT: *J. Iron Steel Inst.*, 1972, **210**, 857.
10. J. P. NAYLOR and P. R. KRAHE: *Metall. Trans.*, 1975, **6**, 594.
11. A. L. TENUTA AZEVEDO and E. GALVAO DA SILVA: *Scr. Metall.*, 1978, **12**, 113.
12. H. K. D. H. BHADESHIA and D. V. EDMONDS: *Metall. Trans.*, to be published.
13. N. C. LAW and D. V. EDMONDS: unpublished research, University of Cambridge.